Reynolds number and Shallow Depth Sloshing

A. Colagrossi
G. Colicchio
INSEAN
00128 Rome, Italy.
a.colagrossi@insean.it

L. Delorme
Eurocopter, ETDAO
13700 Marignane, France
louis.delorme@eurocopter.com

A. Souto-Iglesias
J.L. Cercós-Pita
Naval Architecture Department (ETSIN),
Technical University of Madrid (UPM)
28040 Madrid, Spain.
antonio.souto@upm.es

***Abstract*— The dependence on the Reynolds number of shallow depth sloshing flows inside rectangular tanks subjected to forced harmonic motion is studied in this paper with weakly-compressible SPH. We are interested in assessing the influence of viscous effects on the dynamics of shallow depth sloshing flows by using an SPH solver and by comparing with a Navier-Stokes level-set solver results. The goal of trying to model these viscous flows is compromised by the resolution requested due to their Reynolds number, if boundary layer effects are to be modeled. The convenience and feasibility of the implementation of free-slip and no-slip boundary conditions is also discussed.**

I. Introduction

Sloshing flows are those occurring when free surface waves are generated inside tanks, usually creating significant torque and pressure peaks on the tank due to the impact of traveling waves. These phenomena are of interest for several branches of engineering including marine, aerospace and civil engineering. An abundant literature on sloshing can be found, reviewed in the indispensable book of Prof. Raouf Ibrahim [1], one of the most prominent researchers in the field.

Among the sloshing flows, shallow depth ones are specially attractive due to the structure of the wave systems that are generated under these depth conditions. When dealing with fluids of small viscosity like water, for low frequencies a set of small traveling waves appear. With a small rise in frequency, the train of waves is suddenly transformed into a bore, or hydraulic jump, a distinct step in the water surface [2].

We are interested in assessing the effect on these shallow depth flows of modifications in the Reynolds number due to changes in the physical viscosity. For shallow water flows, previous attempts with SPH codes [3], [4] have been successful in modeling both the bulk flow in terms of the torque [4] and the wave height, even for resonant conditions [3]. Nevertheless concerns on the role of the SPH viscous term [5] on the simulations, when focusing on the time evolution of the bores, have suggested to pursuing the study by checking the flow dependence on the Reynolds number Re, keeping constant all the parameters apart from the physical viscosity. The initial results of such study are presented in this paper. Also, the convenience and feasibility of the implementation of free-slip and no-slip conditions is discussed, paying attention to the characteristic dimensions of the boundary layers (BL) to model, to the computational effort required and to the quality of the results in terms of a correct approximation of the viscous stress term in the SPH momentum equation.

Although comparing experimental data is on our agenda, it has not been possible for this article. Nevertheless, having information from a better established numerical technique, at least for the pre-splashing part of the motion, is also necessary to assess the quality and limitations of the SPH approaches. This reference data has been specifically produced for this study with a Navier-Stokes solver combined with a level-set technique (NSLS) for the tracking of the free surface evolution [6].

The paper is organized as suggested in this introduction: first, the case studies are exposed, documenting the specific flows to resolve as well as the fluid physical properties. Second, the SPH treatment of the viscosity and the BL numerical treatment are discussed. Finally, comparisons with the level set technique data will be provided.

II. Case studies

A. Shallow water flows

The simplest mean to characterize shallow depth sloshing flows is to resort to the dispersion relation for gravity waves in limited depth areas [7].

$$\omega^2 = g\,k\ \tanh\left(k\,H\right) \tag{1}$$

In this expression, g is the gravitational acceleration, H the liquid level, ω is often called the sloshing frequency and k its corresponding wave number. The free surface height function in a two dimensional rectangular container partially filled with liquid can be decomposed in a Fourier series with infinite wave numbers $k_n = n\pi/L$ where L is the tank breadth. If we focus on the first mode, the hyperbolic tangent argument of equation 1 becomes a factor of the ratio H/L. If the depth is great, then the tangent tends to one. If the ratio is for instance 1, the tangent value is 0.996, which means that the effect of the depth on the waves will be very small. In this study a ratio of 0.06 has been chosen, for which the tangent factor is 0.19, which means that this is clearly a shallow water case. The first sloshing frequency, the one corresponding to the first mode will be noted w_1.

The tank is subjected to sway motion with a sinusoidal type excitation. The amplitude A of this motion will be set constant for this study with a value of $A/L = 0.03$. The frequency range for the excitation is $0.5 \leq \omega/\omega_1 \leq 2.0$. The tank length L is 1 meter.

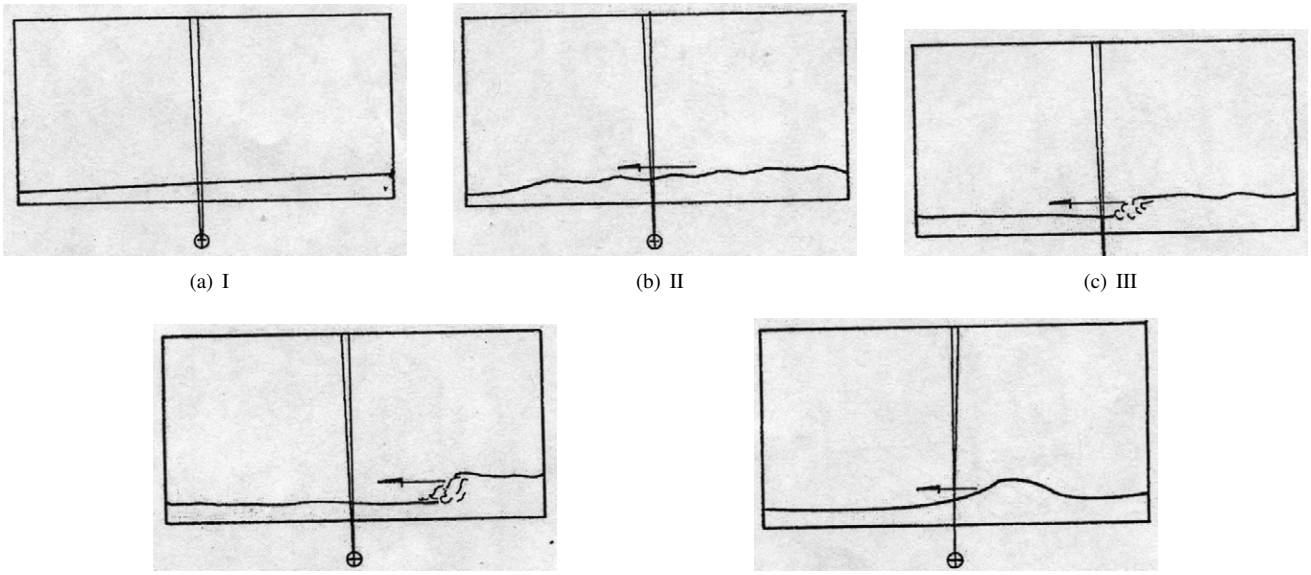

(a) I (b) II (c) III

(d) IV (e) V

Fig. 1. Shallow water free surface paterns. From [2]

As mentioned in the introduction, the shallow water flows than can be found in a sloshing tank either subjected to sway or roll motion are extremely dependent on the excitation frequency. Olsen and Johnsen [2] performed systematic studies dealing with fluids of small viscosity like water. They found that for very low excitation frequency the water follows completely the tank motion, with no lag, and the free surface stays almost flat (figure 1(a)). For slightly higher excitation frequency, a set of small traveling waves appear (figure 1(b)). With a small rise in frequency, the train of waves is suddenly transformed into a bore or hydraulic jump that travels from mid section (figure 1(c)). For even higher frequency, the bore travels from one side of the tank to the other (figure 1(d)). If the frequency keeps rising, the bore becomes a solitary wave (figure 1(e)).

In our particular case, these five scenario can be obtained by changing the excitation frequencies from zero up to the first bifurcation, which occurs for $H/L = 0.06$ around $\omega/\omega_1 \sim 1.4$. The presence of these different propagation patterns highlight the complexity and the non-linearities present in the phenomena.

B. Liquids

Three different liquids have been considered in this study. The first one has been water, with which the concerns on influence of the viscous term on the wave shape and propagation arouse. The second one has been sunflower oil, which is 50 times more viscous than water. The last one was glycerine, approximately 1000 times more viscous than water. The three liquids can be considered newtonian in the range of temperatures that we have operated.

In order to characterize the flows, a consistent definition of the Reynolds number Re has to be considered. The water depth H has been taken as the characteristic length. The magnitude $\sqrt{gH}$ connected with the bore front speed propagation in a dam-breaking problem has been taken as the characteristic velocity.

During the first tests, we thought that the lack of implementation of surface tension effects on the evolution of the wave fronts could be a main cause for the discrepancies, as suggested for instance by Miller [8] and as it will be later discussed (section VI-B). Therefore, the Weber number We was checked, and similar values were obtained for the three liquids. As a consequence, at least initially, the surface tension has been discarded as an influence in this problem. A summary of all the magnitudes can be found in table I. Regarding specifically the Reynolds number, a wide range, from 60 to 50000 is covered with this selection.

Bass et al. [9] considered the influence of viscosity for large amplitude sloshing. They tested $Re > 4000$ to find no influence of this magnitude on the impact pressures. Let's take into account that in the present study we have focused on smaller values of Re.

III. SPH VISCOSITY

Since we are interested in the Re number of the simulation, it is convenient to have a formulation of the SPH equations in which the dynamic viscosity is present. Although some authors [10] have been interested in the past in defining a consistent shear viscosity term in the SPH formalism, Cleary was interested in establishing the relationship between the Monaghan SPH viscous term [11] and the shear viscosity from a practical point of view [12], [13]. Using a gaussian kernel, the Monaghan SPH formalism [11] can be compared, term by term, with the original viscous term in the Navier-Stokes

	ρ	μ	ν	σ	Re	We
Water	998	8.94e-4	8.96e-7	0.0728	51000	500
Oil	900	0.045	5e-5	0.033	920	900
Glycerine	1261	0.934	7.4e-4	0.064	62	700

TABLE I

PHYSICAL PROPERTIES (UNITS SI) OF THE LIQUIDS AND NON-DIMENSIONAL PARAMETERS.
ρ FOR DENSITY, μ FOR THE DYNAMIC VISCOSITY, ν FOR THE KINEMATIC VISCOSITY AND σ FOR SURFACE TENSION.

equations to give an effective kinematic viscosity for the SPH simulation, that Cleary tried to calibrate [14].

His work was completed by Hu and Adams [15], who elegantly devised the connection between the continuum velocity laplacian in the incompressible NS equations and the Monaghan SPH viscous term, using the equally elegant approximation to the second derivatives due to Español etal [16].

The specific expression that will be used in this study for the viscous term is the one from [13].

$$\Pi_{ab} = -8\frac{\mu}{\rho_a\,\rho_b}\,\frac{\mathbf{v}_{ab}\cdot\mathbf{r}_{ab}}{{\mathbf{r}_{ab}}^2+\epsilon\,h^2} \tag{2}$$

where a, b refer to the particles' indexes, $\mathbf{r}_{ab}$, $\mathbf{v}_{ab}$, refer to the difference between positions and velocities respectively, h is the smoothing length, and ϵ is a parameter to avoid any singularity.

For the sake of completeness of the paper, the complete SPH formulation will be the following:

$$\frac{d\rho_a}{dt} = \sum_{b\in\mathcal{N}_a} m_b\,\mathbf{v}_{ab}\,\nabla W_a(\mathbf{r}_b) \tag{3}$$

$$\frac{d\,\mathbf{v}_a}{dt} = \sum_{b\in\mathcal{N}_a} m_b\left(\frac{P_a}{\rho_a^2}+\frac{P_b}{\rho_b^2}+\Pi_{ab}\right)\nabla W_a(\mathbf{r}_b)+\mathbf{g} \tag{4}$$

$$\frac{d\mathbf{r}_a}{dt} = \mathbf{v}_a \tag{5}$$

$$P = \frac{\rho_0\,c_s^2}{\gamma}\left(\left(\frac{\rho}{\rho_0}\right)^{\gamma}-1\right) \tag{6}$$

in which $\nabla W_a(\mathbf{r}_b)$ is the gradient of the a-centered kernel at point b, $\mathcal{N}_a$ is the index set of particle a neighbors regarding the kernel support, m is the mass, P the pressure, ρ_0 the reference density, c_s is the numerical sound speed and $\gamma = 7$. The kernel will be a renormalized Gaussian kernel with a support of $3h$ and $h = 1.33\,dx$ where dx is the typical initial separation among particles.

IV. REYNOLDS NUMBER AND BOUNDARY LAYERS (BL)

A. Reynolds number

When comparing the Cleary viscosity factor(eq. 2) with the Monaghan [11] viscous term, for which abundant analysis in terms of stability are available, the following relation is obtained:

$$\nu \sim \frac{1}{8}\alpha h c_s \tag{7}$$

The α factor should be not less than 0.01, with c_s being 10 times the maximum expected velocity u_{max}, if time integration is expected to remain stable. If it is assumed that $u_{max} \sim 2\sqrt{gH}$, we get that

$$Re \sim \frac{2}{dx} \tag{8}$$

The minimum number of particles for each of the cases in table I, required to expect time integration stability is therefore the following.

	water	oil	glycerine
number of particles	46e6	17e3	60

The water case (46 million particles) cannot be hence tackled with our means, but if we could, probably instabilities in the flow itself would appear due to the onset of turbulence. Nevertheless, the effects of such instabilities would keep basically constrained to the BL area and would not significantly affect the wave patterns. This will be later confirmed (section VI-B) with the comparisons between the experiments and the oil case simulations, which match in what respects to the free-surface shape.

B. Boundary layers (BL)

In order to establish the solid boundary conditions (BC), ghost-particles (GP) have been used. Monaghan [17] showed the accuracy of SPH to model shear in a Couette flow. The boundaries were modeled with fixed fluid particles. These particles can not stand the normal forces needed to stop the fluid particles getting out of the tank in the sloshing case.

When the oil case was run with GP and free-slip BCs, it was found that the dynamics was different to the one obtained with the NSLS solver with no-slip BCs. The numerical Re seemed to be greater, with free surface patterns similar to those typical from water: overturning waves, splashing, etc... These patterns were also obtained with the NSLS solver with free-slip BC. Therefore, the BL have to taken into account.

It seems that in the oil case and even more in the glycerine one, due to their Re number at least in principle both flows should stay laminar. In order to resolve the viscous character of the flow, the momentum transfer from the flow to the solid boundaries has to be, as justified, properly modeled. Properly resolving the proposed flows is not just a question of stability but also of accuracy, and therefore the scales corresponding to the BL have to be estimated in order to define the required resolution to capture the velocity gradients close to the walls.

To simplify the problem of estimating the BL thickness, a steady flow over a flat plate of length H or L has been considered. The Blasius formula for the laminar BL thickness δ will be used, taking into account that the velocity of the bulk

flow U could be of the order of $\sqrt{gH}/2$ because only those belonging to the leading crest would achieve the characteristic value (section II-B).

$$\delta_x \sim \sqrt{\frac{\nu x}{U}} = \sqrt{\frac{2xH}{Re}} \tag{9}$$

For the oil case, the values obtained are $\delta_H \sim 3\,\mathrm{mm}$ and $\delta_L \sim 12\,\mathrm{mm}$. The value of $dx \sim 2\,\mathrm{mm}$ obtained in this case from the stability considerations of section IV-A suggests that it will be very hard to simulate the BL for the oil case. In particular, what was found is that the SPH solver is unstable for this case and it is necessary the use of a periodic rezoning where the particles are redistribute on a regular lattice [18]. The developed rezoning algorithm [19] minimizes the error on the total volume. This means that this error when referred to the total fluid volume remains close to the initial one even after a large number of rezoning events. This characteristic is quite important when dealing with free surface problems.

The use of periodical rezoning introduces numerical noise which in turn affects the accuracy of the SPH solution. For the lowest Re number case (i.e. using glycerine), the BL is thicker and the drawbacks of the periodical rezoning are less evident since the velocity gradients are not so strong as in the oil case.

V. Tangential velocity of the Ghost Particles.

The no-slip boundary condition at a solid-liquid interface is at the very heart of our understanding and intuition of fluid mechanics. There is abundant research ongoing in the field of Micro-fluidics regarding the convenience and physical validity of this condition [20], [21]. We mention this fact to introduce the issue of how no-slip BC will be treated in the present paper with SPH, which, as usually mentioned, mimics molecular dynamics.

In principle the classical Takeda [10] technique of creating GP by mirroring not only the normal but also the tangential velocity was used in this study to implement the no-slip BC. A more naif try of just making equal to zero the tangential velocity of the GP was finally selected to surprisingly find results of the same quality and with less instabilities; actually rezoning was not needed for the low Re for this possibility. We will try now to justify the reason for this behavior.

From equations 2 and 4, the SPH approximation to the divergence of the viscous part of the stress tensor T^ν for a particle of index a can be written as:

$$\langle \nabla \cdot T^\nu_a \rangle = -8\mu \sum_{b \in \mathcal{N}_a} \frac{m_b}{\rho_b} \frac{\mathbf{v}_{ab} \cdot \mathbf{r}_{ab}}{{\mathbf{r}_{ab}}^2 + \epsilon\, h^2} \nabla W_a(\mathbf{r}_b) \tag{10}$$

The frame of reference is now considered centered on the a particle. The expression 10 can be reformulated at a continuous level as:

$$\langle \nabla \cdot T^\nu_a \rangle = -8\mu \int_{\Omega_a} \frac{(\mathbf{v} - \mathbf{v}_a) \cdot \mathbf{r}}{\mathbf{r}^2} \nabla W_a(\mathbf{r}) dV \tag{11}$$

in which Ω_a is the support of the particle a centered kernel function, and dV is the volume element. Considering a Gaussian kernel and using polar coordinates (r, θ):

$$W(r) = \frac{e^{-(r/h)^2}}{\pi h^2}; \quad \nabla W = \frac{\partial W}{\partial r} \mathbf{u}_r; \tag{12}$$

where $\mathbf{u}_r$ is the normalized r direction vector. Equation 13 can be therefore written as:

$$\langle \nabla \cdot T^\nu_a \rangle = -8\mu \int_0^{2\pi} \int_0^{\infty} \frac{(\mathbf{v} - \mathbf{v}_a) \cdot \mathbf{r}}{\mathbf{r}^2} \frac{\partial W}{\partial r} \begin{pmatrix} \cos\theta \\ \sin\theta \end{pmatrix} r dr d\theta \tag{13}$$

Let's consider a divergence free velocity field such as $\mathbf{v} = (u, v) := (y^2/2, 0)$, the fluid domain will be the set $\Omega = \{\mathbf{r}, y > 0\}$, and the solid boundary $\partial\Omega$ will be hence the line $y = 0$ (figure 2(a)). The continuum value of the viscous stress for this velocity field will be constant:

$$\nabla \cdot T^\nu = \mu \nabla^2 \mathbf{v} = \mu \begin{pmatrix} 1 \\ 0 \end{pmatrix} \tag{14}$$

In particular this would be the value at the solid boundary. Since $\mathbf{v}(x, -y) = \mathbf{v}(x, y)$ for this particular velocity field, this is like having the GP with the same tangential velocity as the fluid particles. If the expression 13 is evaluated, it is possible to see that the same value is obtained. This means that the SPH continuum interpolation produces a correct estimation of $\nabla \cdot T^\nu_a$ in this case.

On the contrary, let's define $\mathbf{v}(x, -y) = -\mathbf{v}(x, y)$, which is the equivalent of mirroring the tangential velocity for the boundary particles. In this case, the equation 13 would give an incorrect null value of the viscous stress in the solid boundary. We think now of the particle a as being close to the solid wall (figure 2(d)). The notation is overloaded by writing $y_a = a$, and the origin of the frame of reference is placed at the particle a, overloading again the notation by using y for the new axis ($y_a = 0$). The velocity field in the new system would be:

$$\mathbf{v} = \begin{pmatrix} \frac{y^2}{2} + ay + \frac{a^2}{2} \\ 0 \end{pmatrix}; \quad \mathbf{v}_a = \begin{pmatrix} \frac{a^2}{2} \\ 0 \end{pmatrix} \tag{15}$$

If we set the velocity for the ghost particles as the symmetric (same sign) of the fluid particles (figure 2(d)), the correct answer for the divergence of the stress tensor is again obtained:

$$\langle \nabla \cdot T^\nu_a \rangle = \mu \begin{pmatrix} 1 \\ 0 \end{pmatrix} \tag{16}$$

On the other hand if the velocity of the GP is defined with antisymmetry, the result is incorrect. Midway, if the velocity of the GP is set zero (figure 2), the result is not correct but is better than by the usual antisymmetry. This result is represented in figure 3, in which the stress at the solid boundary for the two last possibilities is shown. The case with zero velocities for the ghost particles gives a better estimate of the stress divergence continuum approximation at the boundary.

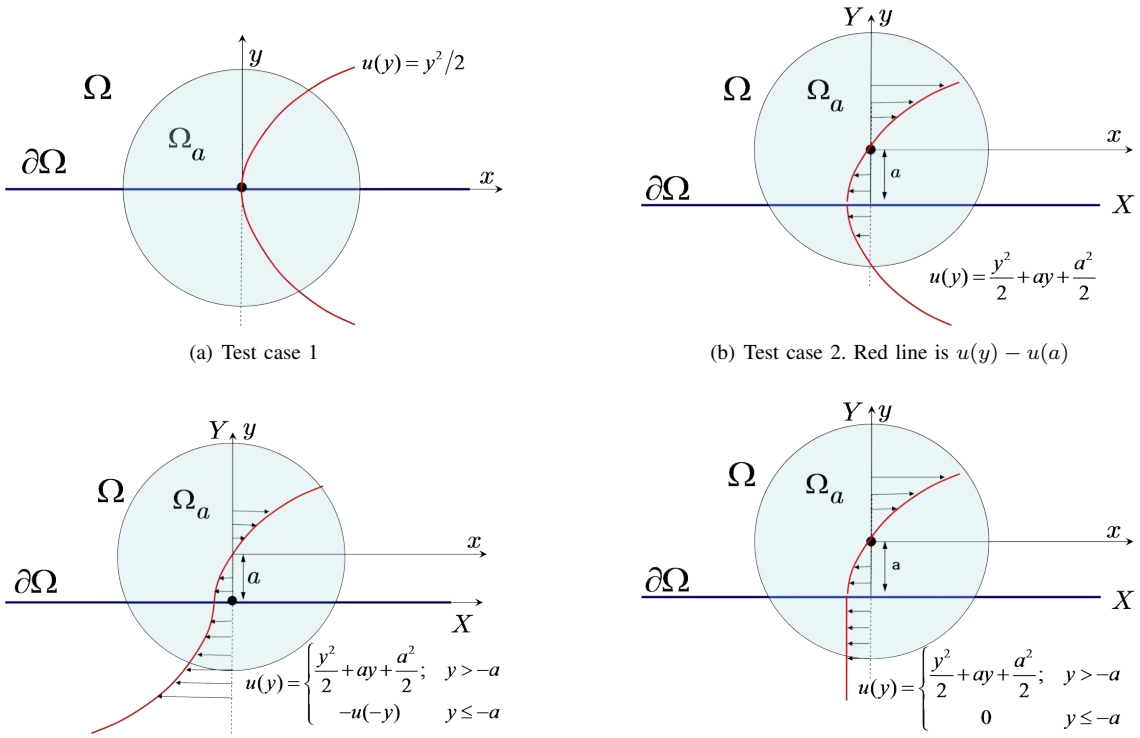

(a) Test case 1

(b) Test case 2. Red line is $u(y) - u(a)$

(c) Test case 2 variant: GP mirroring velocity field.

(d) Test case 2 variant with zero velocity for GP.

Fig. 2. Test cases to check adequate GP tangential velocity

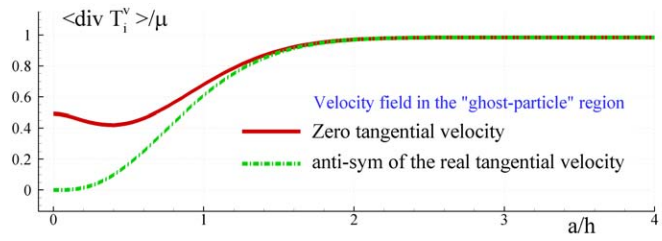

Fig. 3. Stress divergence at the solid boundary

VI. Results

A. General

As exposed in the introduction, although obtaining good quality experimental data to compare with is programmed for next months, it has not been possible for this article. Only previous experimental results obtained taking advantage of a campaign leaded by Dr. Lugni [22] for studying water wave impact related problems have been used. Besides, it is not feasible in the experiments to accurately measure the characteristics of the BL whilst with the numerical outputs all this information can be processed and compared. Therefore, we have resorted to a well established numerical technique to model these shear flows and produce specific reference data for this study. The choice, as mentioned in the introduction, has been a Navier-Stokes solver combined with a level-set technique (NSLS) for the tracking of the free surface evolution [6].

B. Oil, $Re = 920$, free-slip BC

In the oil case, as mentioned, there is both the possibility of comparing with the NSLS solver and with water experiments performed at INSEAN . The oil case is of the order of the highest Re number case than can be run with SPH. It makes sense hence to compare the free-slip oil SPH with the experiments performed with water, since the BL for the water is very thin. In figure 4 the maximum wave height at three different position for a range of frequencies is shown. The position are 1cm from the vertical wall, 5cm from the vertical wall and 50cm from the vertical walls, i.e., the middle of the tank. To evaluate such maximum with the SPH, 10 periods have been considered. Due to the breaking events some dispersion on the data exists and reflect this, the standard deviation of the SPH data has also been plot. On the plot 4(a), the different wave propagation regimes from Olsen & Johnsen [2] as described in section II-A have been marked. The large discrepancies between SPH and experiments for the points around $\omega/\omega_1 \sim 1.2$ are due to the run-up event. In the experiments the run-up jet breaks with large fragmentation while in the simulation it remains attached to the vertical wall and only few particles leave the wall. Conversely, at 5 cm far from the wall (figure 4(b)) the agreement is good.

If we focus on the point $\omega/\omega_1 \sim 0.9$, steep traveling waves form, with the leading crest starting to break as the wave front

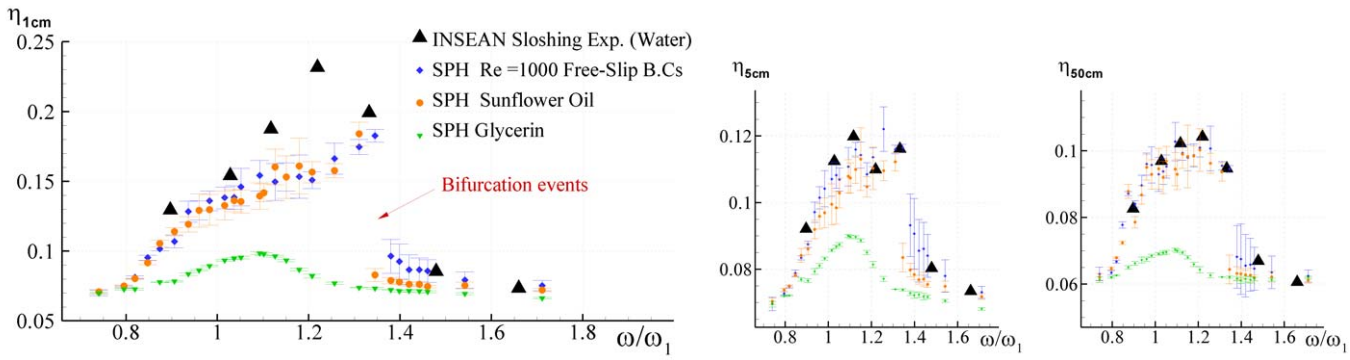

(a) I (b) II (c) III

Fig. 4. Maximum wave height response at 1cm (I), 5cm (II), 50cm (III) from the wall (10 periods)

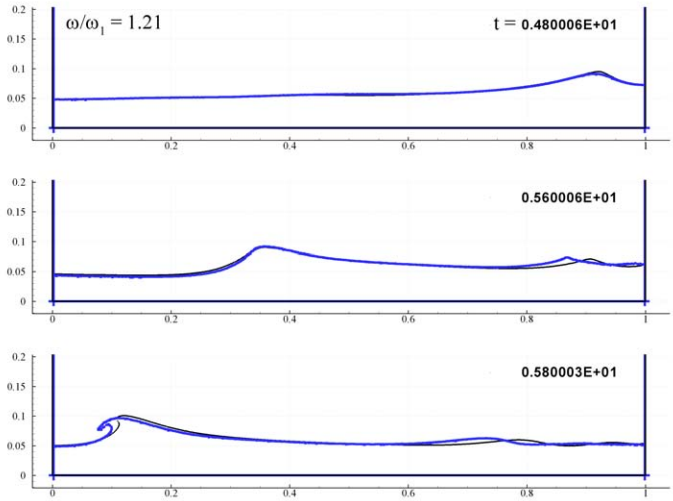

Fig. 6. SPH (blue) vs NSLS (black), $Re = 920$, free-slip BC, $\omega/\omega_1 \sim 1.2$

approaches the vertical wall (figure 5(a)). From this figure, it is quite clear that the surface tension has some effects on the breaking waves. In the experiments, the breaking occurs in a spilling more than in a plunging manner, the latter being the case both in the SPH (figure 5(b)) and in the NSLS simulations. Therefore, even since these surface tension effects should not be neglected, we have done so on the basis of the Weber number, which is similar for the three fluids, as discussed in section II-B. Nevertheless, it could be possible that there is an interaction between viscous and surface tension effects, something that demands a future investigation.

We proceed now with the comparison between SPH and the NSLS for the free-slip case. In figure 6 the wave shape for an excitation frequency equal to $\omega/\omega_1 \sim 1.2$ is shown for both cases. The comparison is good except at the breaking region, where there is a clear lag, with both solvers predicting the breaking event.

C. *Oil,* $Re = 920$*, no-slip BC*

The NSLS solver can provide a good quality solution for the no-slip conditions for this case in order to compare it with the SPH one. For the SPH solver, the no-slip condition has been imposed with zero tangential velocity of the GP, as described in section IV-A. The results are shown in figure 7. The most interesting feature is that the propagation does not lead now to an overturning and wave breaking event. In the bottom figure a zoom of the LS solution is presented. The maps of colors are relative to the vorticity; this allows a direct estimation of the the BL thickness.

A maximum BL thickness of 8mm at a vertical section distance $4H$ from the beginning of the BL has been measured. The velocity just outside the BL is close to $\sqrt{gH}/2$, as had been assumed in section IV-B. The thickness is in good agreement with the Blausis formula, which gives an estimation of 7mm for the BL thickness in these conditions. In the mid plot of figure 7 the SPH vorticity map is shown. A periodic rezoning of the particles has been performed every 0.1 seconds aimed at stabilizing the SPH scheme, as discussed in section IV-B. The SPH solution is affected by some numerical noise due to this rezoning but the thickness of the boundary layer is in a good agreement with the one evaluated by the NSLS solver.

D. *Glycerine,* $Re = 62$*, free-slip BC*

From the analysis with the oil, it is clear the influence of the boundary layers on the flow, and therefore, the convenience of imposing no-slip BC. For the Glycerine, with a quite smaller Re, the interest of studying the flow obtained wit free-slip BC condition is related not so much with its experimental value but with the comparison between a NSLS solution and an SPH one with the classical Monaghan viscous term. With the free-slip assumption, the dominant effect in this quite viscous flow is the presence of the free surface and it is challenging to check how nicely SPH can handle the combination of viscosity and free-surfaces.

After finding in the equivalent case with the oil (section VI-B) that the dynamics was similar but a bit lagged, we did not expect much new in this case. Nevertheless, the differences found have been quite significative (figure 8). The SPH solver provides a steeper wave, but it is in the vorticity field where the differences are more evident. The SPH solution presents

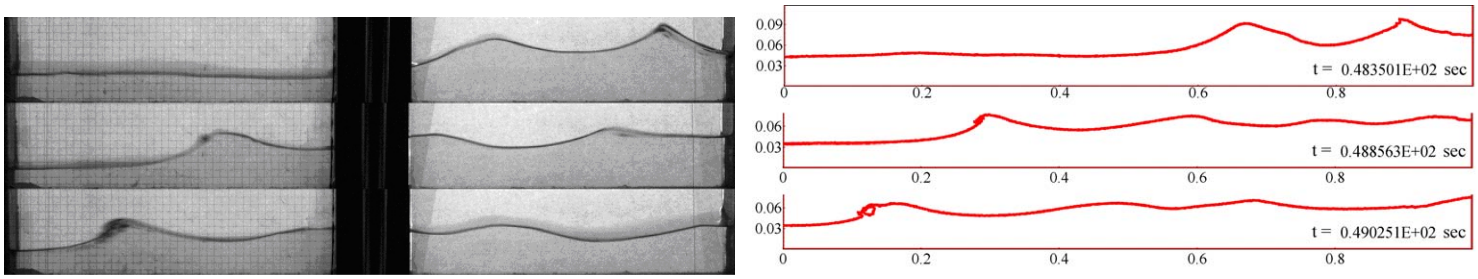

(a) (b)

Fig. 5. Experiments with water (left) and free-slip SPH with oil (right) for $\omega/\omega_1 \sim 0.9$

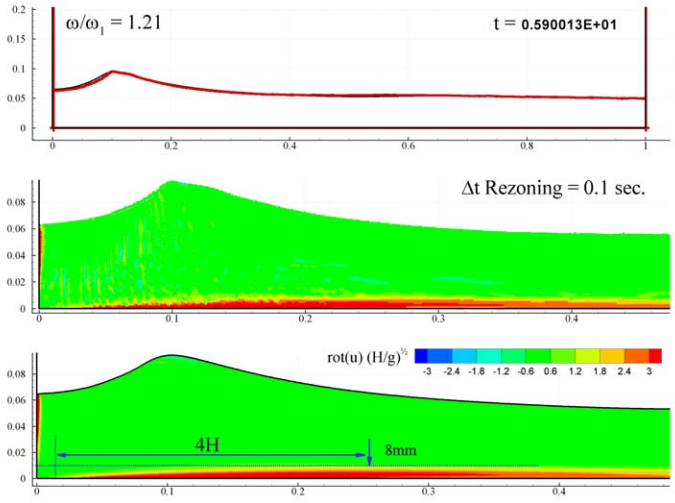

Fig. 7. SPH (mid) vs NSLS (bottom), $Re = 920$, no-slip BC, $\omega/\omega_1 \sim 1.2$. Both (top). Colors refer to vorticity.

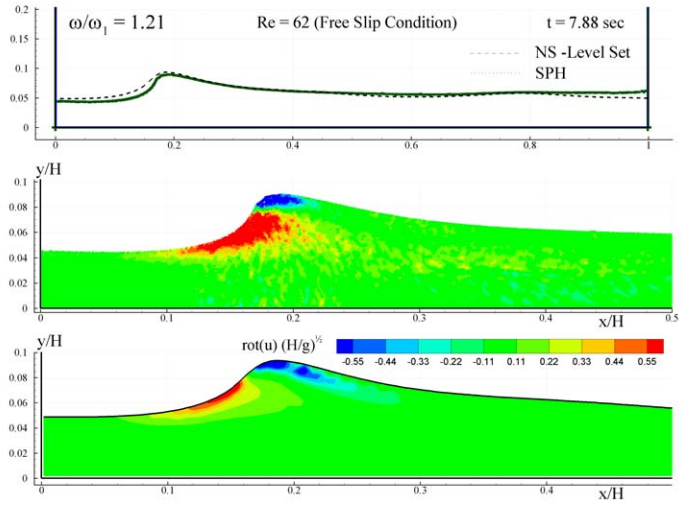

Fig. 8. SPH (mid) vs NSLS (bottom), $Re = 62$, no-slip BC, $\omega/\omega_1 \sim 1.21$. Both on the top one. Colors refer to vorticity.

a stronger vorticiy field than the NSLS solution. This is very interesting because SPH tends to usually perform with more diffusion than Finite Difference schemes. This suggest that we need further study in this case for the understanding of the combined effects of the viscosity models and the free surface effects.

E. Glycerine, $Re = 62$, no-slip BC

After the analysis documented in section VI-C It is evident that for the glycerine (20 times even more viscous than the oil) the only realistic condition is the no-slip one, which has been run both with the NSLS solver and with SPH.

In figure 4 the response operator regarding the wave height for the Glycerine case has been shown. The influence of viscosity on the response is clear from these graphs, reducing the wave height for all the excitation frequencies. The flow is slightly sensitive to the excitation frequency with the maximum response corresponding to $\omega/\omega_1 \sim 1.1$. No overturning waves can be found, the free surface being very smooth (figure 9).

In the same figure, the thickness of the BL can be appreciated. From Blasius expression, a thickness of 30mm was expected mid-tank. This is approximately what has been obtained both with the NSLS solver and with the SPH computations. Two SPH computations have been presented. In the mid-upper one the GP tangential velocity has been set to zero. In the mid-bottom one, the GP tangential velocity of each particle has mirrored the one of the fluid particle [10]. The rezoning algorithm forces that the particles are approximately at least at a distance dx from the boundary. At that distance, as seen in figure 9, the differences between both possibilities in the evaluation of the stress divergence is almost negligible, thus justifying the similitude of both boundary layers. The main shortcoming about the mirroring of the tangential velocity is that the flow is more unstable when no rezoning is used [18].

VII. Conclusions, future work

The dependence on the Reynolds number of shallow depth sloshing flows inside rectangular tanks subjected to harmonic sway motion has been studied with weakly-compressible SPH. The importance of properly imposing the no-slip boundary conditions for these types of flows as well as the difficulties encountered have been highlighted. The different responses

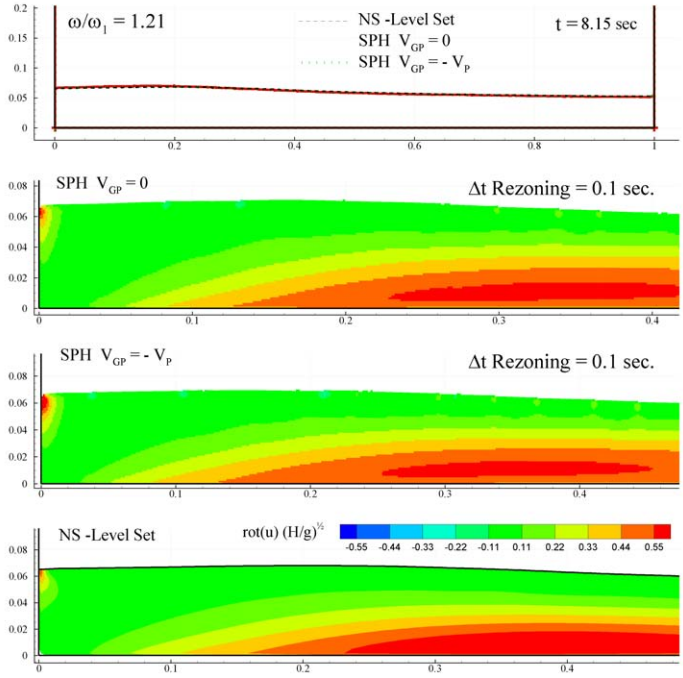

Fig. 9. SPH (mid-upper, mid-bottom) vs NSLS (bottom), $Re = 62$, no-slip BC, $\omega/\omega_1 \sim 1.2$. All on the top one. Colors refer to vorticity.

according to the Reynolds number have been presented by studying a low Reynolds number case and a mid-range one.

No-slip boundary conditions have been imposed with the use of the ghost particle technique. The convenience of mirroring the velocity of the fluid particles to define the ghost particles' velocity, or the possibility of just canceling it has been studied, the latter showing the same quality performance when the solution has been compared with a Navier Stokes Level Set solver one and with less numerical instabilities. A justification of this result based upon the continuum SPH approximation of the stress tensor divergence has been motivated and discussed.

A range of future investigations are suggested from this work. Just to mention a few, the effects of the viscosity on the wave pattern and the capacity of SPH to model them are not yet well understood. The structure of the viscous SPH term which has not only a shear but a bulk viscosity component needs further investigation when modeling sloshing flows. Better and specific experiments aimed at supporting the research are needed. The issue of the ghost particles velocity is not yet completely clear in relation to how it affects the boundary layer profiles, which in turn, for higher Reynolds number, demand multi-resolution techniques, and eventually turbulence modeling. Finally the role of surface tension interactions with viscosity is not yet clear.

ACKNOWLEDGMENT

This work was partially supported by the Centre for Ships and Ocean Structures (CeSOS), NTNU, Trondheim, within the "Violent Water-Vessel Interactions and Related Structural Load" project, and partially done within the framework of the "Programma Ricerche INSEAN 2007-2009" and "Programma di Ricerca sulla Sicurezza" funded by Ministero Infrastrutture e Trasporti.

REFERENCES

[1] R. Ibrahim, *Liquid Sloshing Dynamics*. Cambridge, UK: Cambridge University Press, 2005.

[2] H. Olsen and K. Johnsen, "Nonlinear sloshing in rectangular tanks. a pilot study on the applicability of analytical models," Det Norske Veritas (DNV), Hvik, Norway, Tech. Rep. No. 74-72-5, Vol. 2,, 1975.

[3] M. Landrini, A. Colagrossi, and O. Faltinsen, "Sloshing in 2d flows by the SPH method," in *8th Int. Conf. no Num. Ship Hydrodynamics. Busan. Korea*, Sept. 2003, pp. 1–15.

[4] A. Souto-Iglesias, L. Delorme, L. Pérez-Rojas, and S. Abril-Pérez, "Liquid moment amplitude assessment in sloshing type problems with smooth particle hydrodynamics," *Ocean Engineering*, vol. 33, no. 11-12, pp. 1462 – 1484, 2006.

[5] J. Monaghan, "On the problem of penetration in particle methods," *J. Comp. Phys.*, vol. 82, pp. 1–15, 1989.

[6] G. Colicchio, "Violent disturbance and fragmentation of free surfaces," Ph.D. dissertation, University of Southampton (UK), 2004.

[7] H. Lamb, *Hydrodynamics, Sixth edition*. Cambridge University Press, 1932.

[8] R. L. Miller, "The role of surface tension in breaking waves," in *Proc. 13th Coastal Engineering Conf.* Amer. Soc. Civ. Engrs., 1972, pp. 433–449.

[9] R. Bass, E. Bowles, R. Trudell, J. Navickas, J. Peck, N. Endo, and B. Pots, "Modeling criteria for scaled LNG sloshing experiments," *Trans. ASME*, vol. 107, pp. 272–280, 1985.

[10] H. Takeda, S. M. Miyama, and M. Sekiya, "Numerical simulation of viscous flow by smoothed particle hydrodynamics," *Progress of Theoretical Physics*, vol. 92, no. 5, pp. 939–960, 1994.

[11] J. Monaghan, "Simulating free surface flows with SPH," *J. Comp. Phys.*, vol. 110, no. 2, pp. 39–406, 1994.

[12] P. W. Cleary and J. J. Monaghan, "Boundary interactions and transition to turbulence for standard cfd problems using sph," in *Proc. 6th International Computational Techniques and Applications Conference*, Canberra, 1993, pp. 157–165.

[13] P. W. Cleary, "Modelling confined multi-material heat and mass flows using sph," *Applied Mathematical Modelling*, vol. 22, pp. 981–993, 1998.

[14] ——, "New implementation of viscosity: Tests with couette flows," SPH Technical Note #8, CSIRO Division of Maths and Stats, Tech. Rep., DMS - C 96/32, 1996.

[15] X. Hu and N. A. Adams, "Angular-momentum conservative smoothed particle hydrodynacmis for incompressible viscous flows," *Phys. of Fl.*, vol. 18, pp. 702–706, 2006.

[16] P. Español and M. Revenga, "Smoothed dissipative particle dynamics," *Physical Review E*, vol. 67, no. 2 2, pp. 26 705 – 1, 2003, particle dynamics;.

[17] J. J. Monaghan, "Smoothed particle hydrodynamic simulations of shear flow," *Monthly Notices of the Royal Astronomical Society*, vol. 365, pp. 199–213, 2005.

[18] A. K. Chaniotis, D. Poulikakos, and P. Koumoutsakos, "Remeshed smoothed particle hydrodynamics for the simulation of viscous and heat conducting flows," *Journal of Computational Physics*, vol. 182, pp. 67–90, 2002.

[19] D. Le Touze, private communication, 2007.

[20] E. Lauga, M. P. Brenner, and H. A. Stone, "Microfluidics: The no-slip boundary condition," 2005. [Online]. Available: http://www.citebase.org/abstract?id=oai:arXiv.org:cond-mat/0501557

[21] C.-H. Choi, K. J. A. Westin, and K. S. Breuer, "Apparent slip flows in hydrophilic and hydrophobic microchannels," *Physics of Fluids*, vol. 15, no. 10, pp. 2897–2902, 2003. [Online]. Available: http://link.aip.org/link/?PHF/15/2897/1

[22] C. Lugni, M. Brocchini, and O. M. Faltinsen, "Wave impact loads: The role of the flip-through," *Physics of Fluids*, vol. 18, no. 12, pp. 101–122, 2006. [Online]. Available: http://link.aip.org/link/?PHF/18/122101/1